

PAPER • OPEN ACCESS

Velocity-space analysis of fast-ion losses measured in MAST-U using a high-speed camera in the FILD detector










To cite this article: Lina Velarde *et al* 2025 *Plasma Phys. Control. Fusion* **67** 015024

View the [article online](#) for updates and enhancements.

You may also like

- [Beam-ion losses velocity-space distribution under neutral-beam injection on EAST](#)
S.S. Wang, Z.X. Zhang, J. Huang et al.
- [Experimental investigation of beam-ion losses induced by magnetic perturbations using the light ion beam probe technique in the ASDEX Upgrade tokamak](#)
J. Galdon-Quiroga, L. Sanchis-Sanchez, X. Chen et al.
- [Prompt non-resonant neutral beam-ion loss induced by Alfvén eigenmodes in the DIII-D tokamak](#)
X. Chen, W.W. Heidbrink, G.J. Kramer et al.

Velocity-space analysis of fast-ion losses measured in MAST-U using a high-speed camera in the FILD detector

Lina Velarde^{1,2,*} , J F Rivero-Rodríguez³ , J Galdón-Quiroga⁴ , T Williams⁵,
J Rueda-Rueda⁶ , P Cano-Megías⁷ , R Chacartegui², M García-Muñoz⁴ ,
S Blackmore³, K G McClements³ , L Sanchís⁴ , E Viezzer⁴ , the MAST Upgrade team⁸
and the EUROfusion Tokamak Exploitation team⁹

¹ Centro Nacional de Aceleradores (CNA), Universidad de Sevilla CSIC, J. de Andalucía, Sevilla, Spain

² Departamento de Ingeniería Energética, ETSI, Universidad de Sevilla, 41092 Sevilla, Spain

³ United Kingdom Atomic Energy Authority, Culham Campus, Abingdon, Oxon OX14 3DB, United Kingdom

⁴ Departamento de Física Atómica, Molecular y Nuclear, Universidad de Sevilla, 41012 Sevilla, Spain

⁵ Department of Physics and Astronomy, University of Exeter, Stocker Road, Exeter EX4 4PY, United Kingdom

⁶ Department of Physics and Astronomy, University of California Irvine, San Diego, CA 92186-5608, United States of America

⁷ Max-Planck-Institut für Plasmaphysik, 85748 Garching, Germany

E-mail: lvelarde@us.es

Received 7 August 2024, revised 11 November 2024

Accepted for publication 9 December 2024

Published 24 December 2024



Abstract

A fast-ion loss detector (FILD) was installed for the first time at the mega amp spherical tokamak—upgrade (MAST-U) spherical tokamak during its upgrade in 2021. A new CMOS camera was installed in the MAST-U FILD acquisition system to provide high spatial resolution (1.1 MPx) with an acquisition frequency of up to 3.5 kHz. This camera has enabled the systematic analysis of the velocity-space of the fast-ion losses measured in MAST-U presented in this manuscript. The main parameters that determine the FILD measurement have been analysed to maximise the signal in the detector: the orbit-following code ASCOT predicts an inverse relation between the FILD signal and the probe's relative distance to the separatrix. This prediction has been validated experimentally, enabling the measurement of fast-ion losses in the flat-top phase of the discharge; furthermore, ASCOT simulations show a big impact of the edge safety factor (q_{95}) on the toroidal deposition of the prompt losses, indicating that the signal in the MAST-U FILD can be maximised by running scenarios with $|q_{95}| < 6$. This prediction was validated experimentally by a scan in the toroidal magnetic field. The experimental resolution

⁸ See Harrison *et al* 2024 (<https://doi.org/10.1088/1741-4326/ad6011>) for the MAST Upgrade team.

⁹ See Joffrin *et al* 2024 (<https://doi.org/10.1088/1741-4326/ad2be4>) the EUROfusion Tokamak Exploitation team.

* Author to whom any correspondence should be addressed.



Original Content from this work may be used under the terms of the [Creative Commons Attribution 4.0 licence](https://creativecommons.org/licenses/by/4.0/). Any further distribution of this work must maintain attribution to the author(s) and the title of the work, journal citation and DOI.

of the MAST-U FILD has been evaluated for a typical MAST-U scenario with 750 kA plasma current. The results show that the diagnostic resolution is in the order of 0.5 to 1 degree in pitch angle, and of 1 to 3 cm in gyroradius in current scenarios. A systematic analysis of the velocity-space of the losses shows that the measured gyroradii of the prompt losses match those of the neutral beam injector injection energies within the resolution of the diagnostic. The experimentally measured pitch angles have been compared with ASCOT simulations, and it has been found that the agreement is better for scenarios heated with the on-axis beam, since this beam enables measurements of the magnetic field pitch angle. This analysis has been applied to a discharge where type-III ELM-induced fast-ion losses were measured, showing that the ELMs result in an increase in the FILD signal, and that the losses are coming from passing orbits.

Keywords: fast-ion loss detector, fast-ion losses, spherical tokamaks, velocity-space, ASCOT

1. Introduction

Spherical tokamaks (STs), such as the mega amp ST—upgrade (MAST-U), are an alternative configuration to conventional tokamaks that present better stability [1], and are considered a promising option for future fusion power production plants [2]. In all magnetically confined fusion devices good fast-ion confinement is required for optimum plasma performance, as these particles represent an important source of heating and current drive [3]. MAST-U is heated by two neutral beam injectors (NBIs), constituting the only sources of confined fast ions in this tokamak. Unlike in MAST, where both beams were on-axis, one of the NBIs has now been raised 0.65 m above the midplane, in order to provide off-axis heating and mitigate plasma instabilities driven by high radial gradients in the fast-ion distribution function [4]. The current layout of the injectors—on-axis beam, south–south (SS), and off-axis beam, south–west (SW) – can be observed in figure 1. In MAST-U, the two NBIs are super-Alfvénic, i.e. the speed of the neutrals they inject is higher than the Alfvén velocity of the plasma in this device. Understanding the behaviour of fast ions in these conditions is not only important for present days tokamaks, but for future devices like ITER, where the NBIs and fusion reactions will also provide super-Alfvénic fast-ion distributions. This results in the excitation of a wide variety of Alfvén instabilities, that are susceptible of driving fast-ion losses [5] and damaging plasma facing components, which will not be tolerable in future burning plasmas [6].

In order to study these supra-thermal particles, MAST-U is equipped with a set of diagnostics that allow an in-depth analysis of the confined fast-ion distribution, but with limited information about their losses [7–10]. To complement this set, a scintillator-based fast-ion loss detector (FILD) [11–13] was installed during the upgrade of the machine. This diagnostic studies the behaviour of fast ions that lose confinement, resolving their velocity-space and the frequency of the fast-ion loss fluctuation. FILD is the most widespread diagnostic to measure fast-ion losses in magnetically confined plasmas, being used in different tokamaks such as JET [14–16], ASDEX upgrade [13], DIII-D [17], and in the future in JT60-SA [18], as well as in stellarators, such as Wendstein 7-X [19, 20]. Scintillator-based FILDs, like the one installed in

MAST-U [21], act as a magnetic spectrometer, collimating the lost supra-thermal ions onto a scintillator plate that is mounted on a probe and placed near the plasma. Depending on the position where the ions hit the plate, it is possible to resolve their velocity-space distribution on the time scales of the wave-particle interaction [11]. FILDs acquisition systems are usually comprised of a ‘fast’ camera, that provides high temporal resolution, enabling the analysis of the frequencies correlated with the losses, and a ‘slow’ camera, providing high spatial resolution of the scintillator plate in order to resolve the velocity-space of the lost supra-thermal particles. The two cameras simultaneously measure the light emitted with the help of a beam splitter.

The MAST-U FILD was designed to operate in the 2 mA plasma current scenario that was foreseen for the MAST upgrade operation [21], which has not been achieved yet. Nonetheless, the FILD rotary and reciprocating system has shown to be reliable and compatible with the existing MAST-U scenarios, with plasma currents up to 750 kA [22]. Since the start of the MAST-U experiments, the FILD has contributed to a wide variety of fast particle experiments, summarised in [23], including the detection of fast-ion losses induced by fishbones, neoclassical tearing modes and Alfvén eigenmodes. In this manuscript, the experimental resolution of the diagnostic will be explored for the current MAST-U reference scenario of 750 kA, where the gyroradii measured by FILD are double than foreseen during the design phase. A systematic analysis of the velocity-space of the fast-ion losses measured in MAST-U with each of the beams is performed for the first time here. This analysis has been enabled by the installation of a new high-resolution camera, as will be discussed later in section 2, and represents a crucial step for future fast-ion studies in MAST-U. Furthermore, the commissioning of the diagnostic has been performed by analysing the parameters that dominantly affect the FILD measurements, i.e. the radial position of the diagnostic and the safety factor. The impact of these parameters on the FILD signal has been previously documented in other machines: in ASDEX upgrade, FILD4 is located behind other plasma facing components (protection limiters), meaning that a minimum insertion is required [24]; in JET, the dependence of the FILD signal has been compared for different poloidal and radial positions of the Faraday cups,

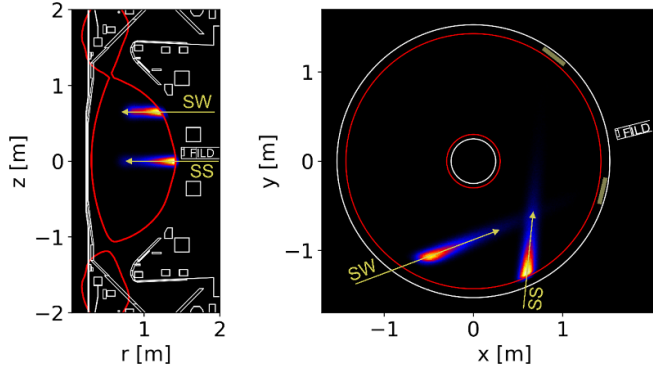


Figure 1. Poloidal (left) and toroidal (right) cross sections of MAST-U, showing the fast-ion birth profiles of the on-axis (SS) and off-axis (SW) beams, along with the wall and FILD probe (white) and the separatrix (in red). The FILD radial position in the toroidal cross section is arbitrary, indicating the toroidal position of the probe. The approximate position of the beam dumps is shown in light yellow.

and for different plasma scenarios [14, 25]; in DIII-D, it was observed that the FILD signal tracks the plasma q profile evolution when prompt losses are being measured [26]. The goal of the analysis presented in this manuscript is to provide a clear reference for the MAST-U FILD operation, both in terms of positioning and plasma parameters, and to broaden the understanding of FILDs operation in STs. Therefore, the text is organised as follows: in section 2, the MAST-U FILD set-up is introduced, and the new camera installed is described. In section 3, the optimisation of the FILD signal with respect to the probe radial position is reported. In section 4, the dependence of the fast-ion loss distribution on the plasma safety factor is analysed, showing the important effect that it has on the FILD signal. Once the effect of the main parameters has been examined, the velocity-space of the fast-ion losses measured is inferred and benchmarked against numerical predictions in section 5. This analysis has also been applied to a discharge where type-III edge localised modes (ELMs)-induced fast-ion losses were measured for the first time, as it is shown in section 6. Finally, in section 7, the results are summarised and discussed. Please note that deuterium plasmas were used for all the analyses presented in this manuscript.

2. FILD set-up at MAST-U

The MAST-U FILD includes a reciprocating system that allows the probe's radial position to be adjusted within a $R = [1.45, 1.60]$ m range (for reference, a typical position of the separatrix is 1.38 m) on a shot-to-shot basis, similar to the systems in ASDEX Upgrade and DIII-D. Additionally, it incorporates an innovative feature, as it is mounted on an angularly actuated mechanism, enabling the orientation of the probe head to be adapted to scenarios with a wide range of safety factor values at the edge (q_{95}). This is a relevant characteristic in a spherical tokamak, where the q profile can vary considerably between different scenarios. A typical radial position of

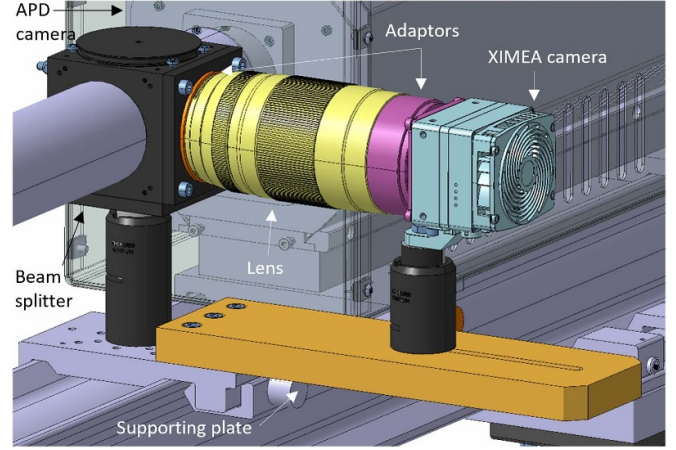


Figure 2. CAD of the XIMEA camera (in light blue) and the designed mount installed in the MAST-U FILD.

the FILD detector (1.48 m) is also shown in the poloidal cross-section in figure 1, whereas the toroidal cross section shows its toroidal position, with an arbitrary radial position. As it can be observed, FILD is located slightly above the midplane ($z = 0.159$ m), and between the two beam-dumps shown in light yellow ($\phi_{\text{FILD}} = 15$ degrees), in a privileged position to measure the prompt losses (particles that get lost before completing one poloidal period) coming from both beams, as will be discussed later in section 4.

In the scope of this work, the existing ‘slow’ camera installed in the MAST-U FILD was upgraded for the second (2022/2023) campaign: a XIMEA CMOS camera was installed, providing spatial resolution of up to 1.1 Mpx, and improving the acquisition frequency from 23 Hz to up to 3.5 kHz and the exposure time from 40 ms down to $1 \mu\text{s}$. The low sampling rate of the old camera made it impossible to resolve the velocity-space of the losses at the typical times of the plasma instabilities in MAST-U. Therefore, the new camera has enabled the systematic analysis of the velocity-space of the losses presented in this manuscript, broadening the possibilities for the physics studies that can be performed using the MAST-U FILD diagnostic, including the analysis of type-III ELMs that will be presented in section 6.

The new set-up is shown in figure 2, where a computer aided design model of the XIMEA CMOS camera installed in the FILD data acquisition system is displayed. To achieve high temporal resolution, this FILD includes an avalanche photodiode (APD) camera, APDCAM-10G, with a sampling rate of up to 4 MHz, allowing the analysis of fast-ion losses coherent with magnetohydrodynamic (MHD) instabilities at frequencies up to 2 MHz.

3. Signal dependence on distance to separatrix

For the commissioning of the reciprocating system, understanding the dependence of the particles flux reaching the scintillator on the position of the detector was the first crucial step. To this end, predictive simulations were performed

using the orbit-following code ASCOT [27] to better understand the behaviour of the losses and their dependence to the probe head's position. ASCOT is a Monte-Carlo code that solves the kinetic equation for fast-ions and minority species in magnetically confined plasmas to describe the full orbit of the particles. This is important, as the gyro-centre approximation is not accurate for fast ions in STs such as MAST-U, due to the large Larmor radii of these particles relative to the magnetic field scale length [28]. Therefore, all simulations presented in this manuscript use the full-orbit approach. To calculate the ionisation distributions of the neutrals injected, a realistic model of the MAST-U NBIs and the parameters used for each discharge, in terms of voltage and power, are employed. This model of the NBIs was included in the latest version of the BBNBI code [29], a complementary tool that is generally run coupled to the ASCOT code, in order to produce the markers that are then used as input of the ASCOT simulation. Furthermore, a realistic 3D model of the MAST-U wall, that includes the FILD detector, and allows for adjustments in its radial position and orientation, is employed. Coulomb collisions are not included in the simulations performed, as only prompt losses are of interest to the analysis presented here. The simulations use experimental data from discharges #45216 and #45383: equilibrium reconstruction was produced using EFIT++ [30] (constrained only with magnetic measurements for the standard reconstruction), and density and temperature profiles were obtained from the Thomson scattering (TS) [31] and charge exchange recombination spectroscopy (CXRS) [32] diagnostics. These profiles are needed to calculate the ionisation distribution with BBNBI.

The discharges simulated in this section were selected due to their similar parameters, being double-null plasmas with a plasma current (I_p) of 750 kA, a toroidal magnetic field at the magnetic axis (B_t) of 0.6 T and similar heating schemes, using both on-axis and off-axis beams with injection energies around 65 keV and 1.5 mW of power. Although in #45383 the beams were not used simultaneously, they have both been included in the ASCOT simulations to allow a comparison between the two discharges. The relevant difference between them for this analysis was the plasma outer radius at the mid-plane, that was set to 1.40 and 1.38 m, respectively, via outer-radius feedback control. In the simulations, the radial position of the FILD detector was scanned to analyse the change in the signal intensity for the different positions. The simulations show that the number of markers reaching the detector is comparable for the two discharges when the separation between the detector and the plasma outer radius is the same, as can be seen in figure 3. The results also show that there is a clear relation between the number of markers reaching the diagnostic and the distance between the probe head and the separatrix. No thresholds are shown in the inverse relation between the relative distance and the intensity of the signal, indicating that no other plasma facing component is obstructing the FILD detection [24, 33, 34].

A scan in the plasma outer radius was performed experimentally (#46942) to verify these results. This was done by fixing the position of the FILD detector at 1.5 m, and scanning

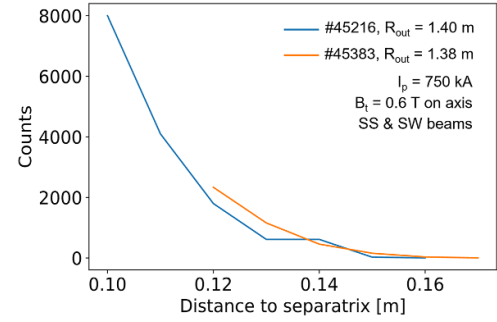


Figure 3. Number of markers reaching the probe head versus its distance to the separatrix in the ASCOT simulations for two discharges with different plasma outer radius.

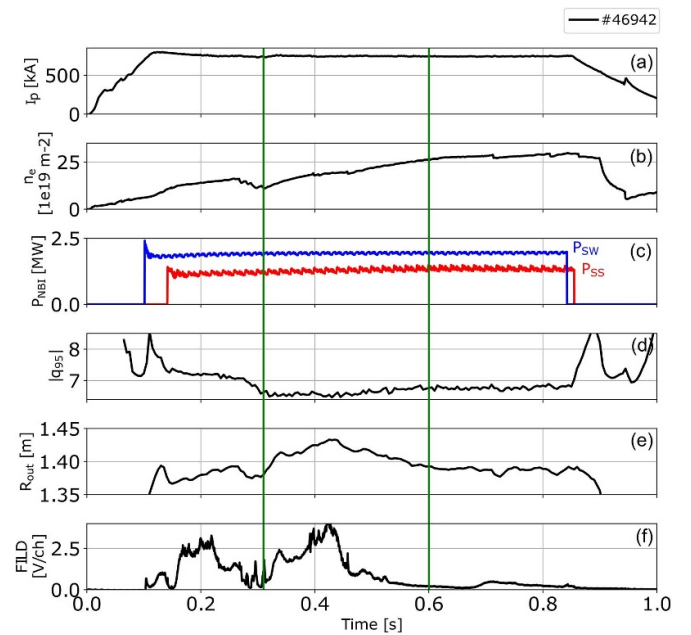


Figure 4. Time traces for shot #46942, showing the evolution throughout the discharge of the plasma current (a), line-integrated electron density (b), NBI power (c-SW in blue, SS in red), edge safety factor (d), outer radius during the scan (e), and integrated FILD signal (f). Raw signal in volt is plotted for FILD. The time window of the R_{out} scan is marked by the green vertical lines.

the outer radius (R_{out}) of the plasma from 1.38 to 1.43 m, and then decreasing it back to 1.38 m. This H-mode shot was carried out with similar parameters to the ones used for the simulations: plasma current of 750 kA, toroidal magnetic field at the axis of 0.66 T and both SS and SW beams on simultaneously. The relevant time traces of the discharge are displayed in figure 4: plasma current, with a flat-top starting from 0.13 s and ending at 0.8 s; line-integrated electron density, which was not feedback-controlled and hence kept increasing during the discharge as a result of recycling and good plasma confinement, as it is typical in MAST-U H-mode plasmas; input power of each of the beams, where the SW is shown in blue and the SS in red; and edge safety factor. Finally, the traces of the outer radius and the integrated signal measured by the FILD

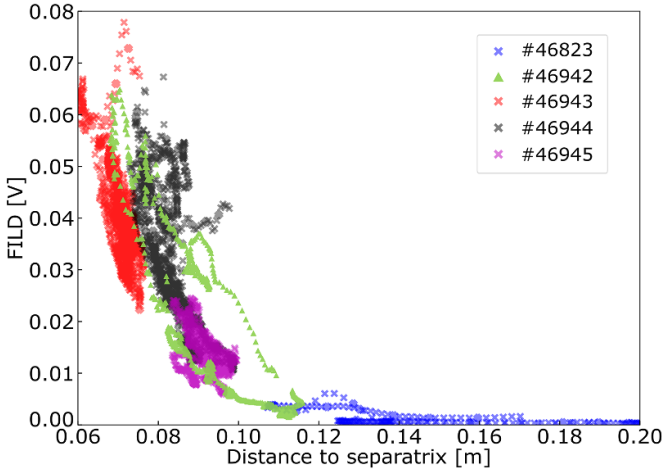


Figure 5. Experimental signal in the FILD detector versus its distance to the separatrix for 5 discharges with $I_p = 750$ kA, $B_t = 0.6$ T at the axis and both beams on simultaneously, but different FILD positions. The green points show the signal measured during the R_{out} scan, #46942.

detector with the APD camera are displayed: the outer radius evolves as previously described, with the time window of the scan marked by the green vertical lines, including an initial phase from 0.31 to 0.42 s where it was increased, and the descending phase from 0.42 to 0.6 s. As expected, the FILD signal shows a similar evolution to that of the outer radius, increasing when the plasma is closer to the probe.

The evolution of the FILD signal with respect to the probe's distance to the separatrix for this shot is shown in figure 5 in green, along with a base reference from shot #46823, in dark blue, and signals from three other shots. The green triangles correspond to the outer radius scan (from $t = 0.31$ s to $t = 0.80$ s). As can be observed in this figure, the FILD signal has an inverse dependence on the distance to the separatrix. Therefore, the prediction made using the ASCOT code has been matched, showing that the signal of the MAST-U FILD depends on the relative distance between the probe head and the outer radius of the plasma, with no thresholds due to limiters or any other in-vessel elements.

Following this outer radius scan, the succeeding discharges (#46943, #46944 and #46945) were designed to confirm this behaviour, now scanning the relative distance to the separatrix by fixing both the FILD probe position and the outer radius during the entire pulse: $R_{FILD} = [1.49, 1.49, 1.50]$ m and $R_{out} = [1.42, 1.41, 1.41]$ m, resulting in a relative distance of 0.07, 0.08 and 0.09 m, respectively for each discharge. The results from these discharges are also displayed in figure 5, clearly showing how they all match the curve described by the R_{out} scan from shot #46942. Furthermore, a second lesson-learned can be extracted from this figure, as it shows that there is a distance below which FILD starts measuring prompt losses: for this type of scenario and heating, FILD needs to be inserted closer than 10 cm in order to achieve a stable signal of prompt losses during the entire discharge. Although this number has

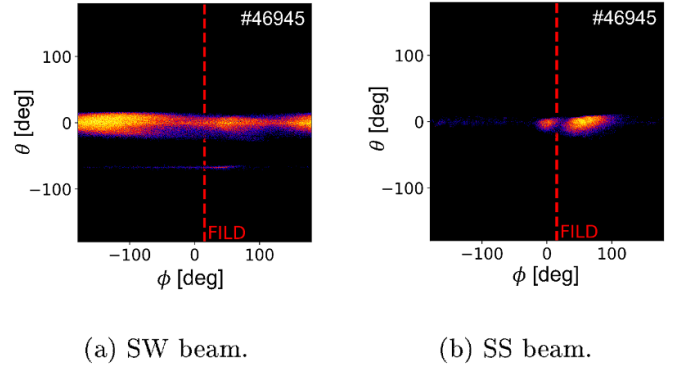


Figure 6. Simulated distribution of fast-ion losses on the wall for the two beams, in the toroidal vs poloidal direction, and FILD toroidal position in dashed red line. The midplane is located at $\theta = 0$ degrees.

been observed to vary slightly, depending on the plasma current and heating power, it has proven to be a solid reference for the FILD positioning in subsequent experiments.

4. Sensitivity to safety factor q_{95}

As previously introduced, the commissioning of the diagnostic continues with the analysis of the effect of the edge safety factor ($\Psi_{pol} = 0.95$, q_{95}) on the fast-ion losses. The understanding of how this parameter evolves is crucial in STs, like MAST-U, as these are more compact machines than conventional tokamaks, with a lower aspect ratio and a typically higher elongation [35]. This translates into a more pronounced variability of the q profile at the edge, affecting the deposition pattern of the fast-ion losses on the wall, and hence the FILD measurement. For this analysis, the on-axis (SS) and off-axis (SW) beams have been modelled and simulated with ASCOT separately. Note that, as in the previous section, all simulations performed here have used experimental data for the kinetic profiles, and the equilibrium reconstruction from EFIT++, in this case constrained by motional stark effect (MSE) measurements of the magnetic field pitch [36], as the results rely on an accurate reconstruction of the q_{95} parameter. On the other hand, a rotationally symmetric 2D wall has been used in this analysis for simplicity.

The results in figure 6 show the distribution of the prompt losses on the wall for shot #46945, for the two beams separately. This distribution is presented as a function of the toroidal angle (ϕ) versus the poloidal angle (θ), where the midplane would be $\theta = 0$ degrees and the upper and lower X-points are usually around $\theta = \pm 100$ degrees. It can be observed that the SW prompt losses (figure 6(a)) are distributed toroidally all along the wall, while the SS prompt losses (figure 6(b)) are localised at a specific area in the toroidal direction, close to the FILD detector (whose toroidal position is shown by the dashed red line, and is located close to the midplane). Although the results from only one discharge are displayed here, this is the typical behaviour that has been found in the many discharges simulated with ASCOT, and it is most likely due to the

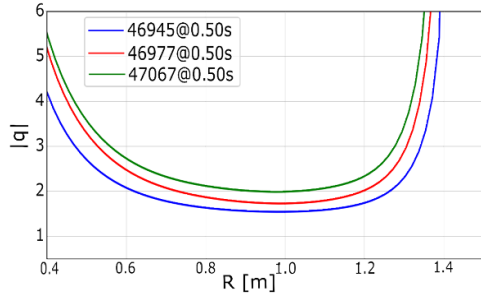


Figure 7. Radial profile of the safety factor for discharges #46945, #46977 and #47067.

topology of the orbits: the particles produced by the SS beam are generally trapped (or close to the trapped-passing boundary), while those produced by the SW beam are predominantly passing, which results in a more free movement in the toroidal direction and consequently a spread distribution on the wall. Hence, the sensitivity of the FILD signal to the q_{95} parameter will be investigated here by focusing on the SS beam, which produces more localised losses, making it easier to isolate the effect that this parameter has on the deposition pattern of the prompt losses. To this end, ASCOT simulations have been performed to scan the effect of the q_{95} , using discharges with plasma current $I_p = 750$ kA and different values of the current applied to the toroidal field coils, I_{TF} . This change in the toroidal magnetic field modifies the helicity of the plasma, directly affecting the q_{95} :

- #46945, $I_{TF} = 100$ kA ($B_t \approx 0.60$ T at the magnetic axis), $|q_{95}| = 6.1$
- #46977, $I_{TF} = 110$ kA ($B_t \approx 0.66$ T at the magnetic axis), $|q_{95}| = 7.6$
- #47067, $I_{TF} = 120$ kA ($B_t \approx 0.70$ T at the magnetic axis), $|q_{95}| = 8.4$

The radial evolution of the safety factor for the selected discharges is shown in figure 7, for the time instant used for the simulations performed with ASCOT. Figure 8 shows the simulated toroidal distribution of the SS-beam losses for the different discharges analysed. The two peaks displayed for each shot mainly correspond to full (right) and half (left) beam energy losses. From this figure, it can be observed that the q profile at the edge has a great impact on how the prompt losses are deposited on the wall. As would be expected, when the safety factor increases, the field line helicity decreases, and the particles travel a longer path before reaching the wall. In this case, the neutrals are being injected at around $\phi = -60$ degrees and the ionised particles travel counter-clockwise—in the positive ϕ direction. Accordingly, simulations predict that, when lowering the $|q_{95}|$ (increasing the helicity of the field lines), the SS losses are localised closer to the FILD probe head, as they travel a shorter path before reaching the wall. This would indicate that, to position the prompt losses at the FILD head, and hence maximise the signal in the detector, it would be necessary to run scenarios with higher plasma current, or with lower magnetic field, in order to achieve an

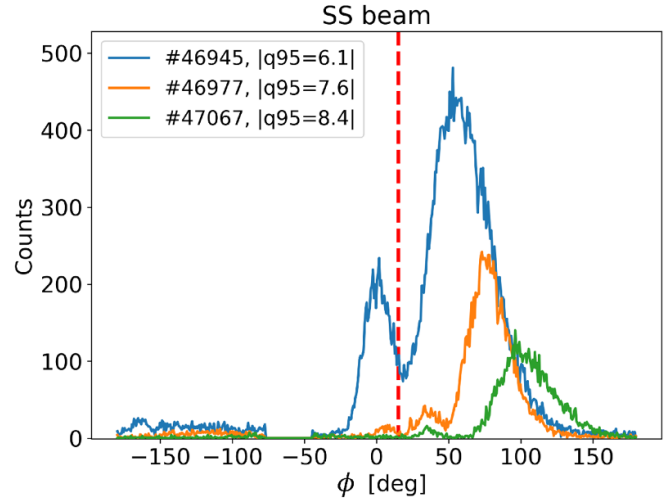


Figure 8. Distribution of the SS-beam fast-ion losses in the toroidal direction of the wall, for discharges #46945, #46977 and #47067. The dashed red line marks the FILD toroidal position.

optimum configuration where the particles are deposited toroidally around the FILD position.

To validate these simulations, an experiment was designed (#48221) where the toroidal magnetic field was ramped down from 0.42 s onwards, allowing us to scan the q_{95} in one single discharge. This descent in the magnetic field leads to a decrease of the edge safety factor, which, according to the simulations, would deposit the SS prompt losses closer to the FILD detector. This should be translated into an increase of the FILD signal.

The time traces of shot #48221, along with the magnetics spectrogram showing the MHD activity, are displayed in figure 9. The plasma current for this shot was set to $I_p = 750$ kA and the SS NBI power to 1.5 mW, with the beam turned off at $t = 0.54$ s, as marked by the green line. The time traces show the evolution throughout the shot of the line-integrated electron density (a); the D_α emission (b); the toroidal magnetic field at the axis (c), with an applied current to the toroidal fields at the beginning of the ramp ($t = 0.42$ s, as marked by the blue line) of $I_{TF} = 110$ kA, resulting in $B_t \approx 0.65$ T at the axis; and the edge safety factor (d). Finally, the traces of the signal measured by the FILD detector with the APD camera (e) and the neutrons measured by the fission chamber [37] (f) are displayed, along with the magnetics spectrogram (h). As can be seen in the FILD panel, when the ramp starts, the signal measured by FILD shows the expected increase. This increase is not correlated to an increase in the MHD activity, as manifested in the bottom panel (however, the brief decrease in the FILD signal at around 0.51 s itself is related to a decrease in the MHD activity). During this time window, it is also possible to observe an interesting sawteeth-like behaviour in the magnetics spectrogram, correlated with punctual drops in the fast-ions losses and peaks in the neutrons measured by the fission chamber. It was not possible to perform this ramp below 90 kA in the toroidal field coils ($B_t \approx 0.56$ T at the axis) due to a mode locking and causing a disruption.

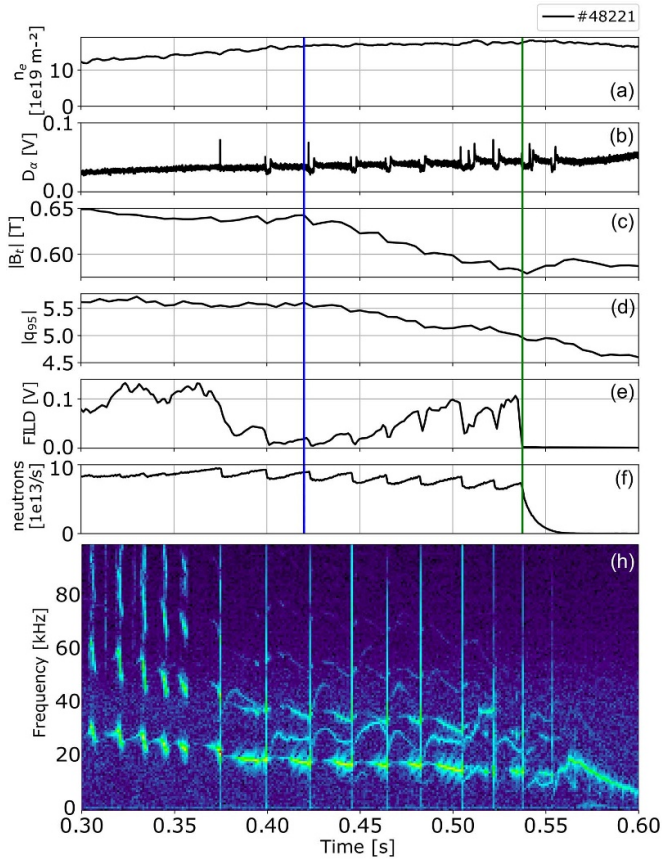


Figure 9. Time traces for shot #48221 of the line-integrated electron density (a), D_α emissivity (b), toroidal magnetic field at the axis (c), edge safety factor (d), integrated FILD signal (e), neutrons (f) and magnetics spectrogram (h). The blue line marks the beginning of the toroidal magnetic field ramp and the green line marks the time instant where the beam is turned off.

5. Velocity-space analysis

In this section, the velocity-space of the fast-ion losses is resolved for the first time in MAST-U. As briefly introduced earlier, FILD consists of a scintillator plate where the lost collimated ions collide, emitting light. The new CMOS camera installed at the MAST-U FILD provides a view of the entire scintillator, capturing the evolution of the position where the losses hit the plate at a frequency of up to 3.5 kHz. This position in the scintillator can then be translated to velocity-space variables: gyroradius ($r_L = \frac{mv_\perp}{qB}$) versus pitch angle ($\lambda = -\arccos(v_\parallel/v)$, being v_\parallel the particle velocity projected along the magnetic field direction) using the recently updated orbit-tracing code FILDSIM [38–40]. The terms ‘pitch angle’ and ‘pitch’ will be used univocally in this manuscript. A collection of ions, with different pitch angles and gyroradii, are traced from the pinhole in the FILD head to the scintillator, under a 3D electromagnetic field using the Boris’ leap-frog algorithm [41, 42]. Then, the position where the ions corresponding to each pitch angle and gyroradius hit the plate is collected in a grid referred to as strike map, that translates scintillator coordinates (pixels in the camera) into velocity-space coordinates. It is important to note that the finite size of the

collimator used to collimate the ions results in a finite width of the distributions, as will be further discussed later. These strike maps depend on the relative orientation between the magnetic field and the probe head. When analysing the FILD signal from a discharge, this orientation is calculated for each time instant, and the corresponding strike map is generated.

The experimental resolution of the diagnostic, defined as the standard deviation of the instrument function, will be first explored to enable the first analysis of the velocity-space of fast-ion losses in MAST-U. For an easier understanding of the results, it is more convenient to first analyse discharges where only prompt losses are being measured, since the measured energy should be equal to that of the injection energy used with the NBI, within the resolution of the diagnostic, and it should be possible to reproduce the experimental results with ASCOT simulations, using the experimental kinetic profiles and reconstructed equilibrium. To this end, in the absence of fully MHD-quiescent scenarios in the MAST-U FILD database, the discharges with the most MHD-quiescent time windows have been selected. However, as it will be discussed later, there is still some MHD present in them. The velocity-space analysis will be done for two different discharges, that used either the SS beam only or the SW beam only, so the losses coming from each of the beams can be isolated and better characterised.

5.1. Diagnostic resolution

The MAST-U FILD instrument response [40] (essentially, a probability distribution function) for a typical alignment of the FILD head with the magnetic field can be calculated for both variables of the velocity-space previously defined: gyroradius and pitch angle. The instrument response has been obtained following 5 million markers for a set of 16 different values of r_L , ranging from 3.5 to 21 cm (~ 5 to 182 keV for a typical magnetic field at the FILD head, 0.415 T), and a set of 13 values of λ , ranging from 25 to 85 degrees, a total of 1040 million markers. This takes less than 1 h using the new FILDSIM code. Figure 10(a) shows the instrument function in pitch angle for a typical value of the gyroradius, 13 cm, while figure 10(b) shows the instrument function in gyroradius for a typical value of the pitch angle, 50 degrees. It is observable here that the dispersion in the measurement becomes wider at higher gyroradii due to the finite size of the pinhole and slit used to collimate the ions, as they have a less collimating effect for larger gyroradii. The resolution (standard deviation) in pitch angle and gyroradius for the typical ranges measured experimentally with the MAST-U FILD is shown in figures 10(c) and (d). By looking at the specific case described above, with $r_L = 13$ cm and $\lambda = 50$ degrees, this would mean a resolution of approximately 1.4 cm in gyroradius and 0.4 degrees in pitch angle.

5.2. Velocity-space analysis of prompt losses

As was previously introduced, two one-beam discharges were selected for the analysis of the velocity-space. In the absence of MHD-quiescent scenarios in the FILD database, these

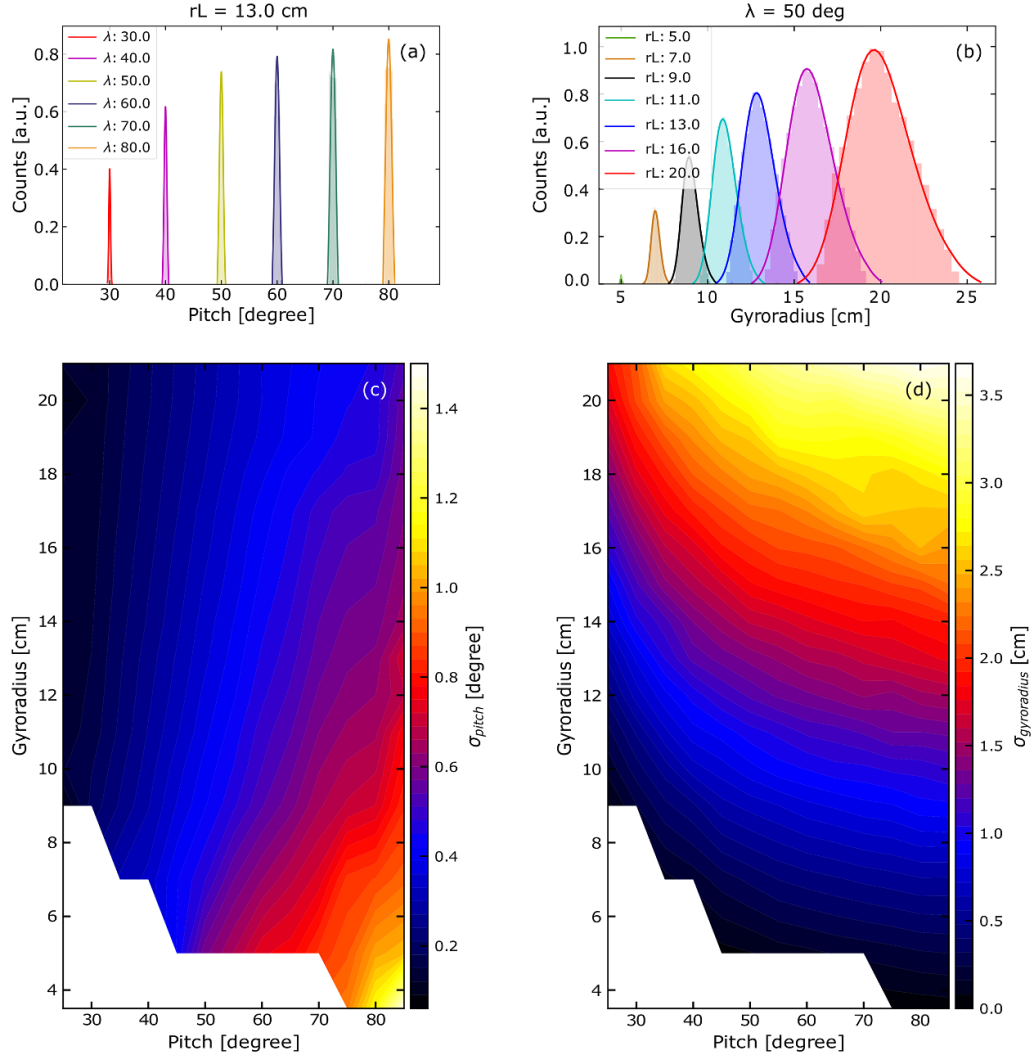


Figure 10. Instrument function of the MAST-U FILD in pitch (a) and gyroradius (b), for $r_L = 13$ cm and $\lambda = 50$ degrees, respectively. Resolution of the diagnostic in pitch (c) and gyroradius (d) for typical measuring ranges of the MAST-U FILD.

two discharges were selected because they present time windows where the magnetics spectrograms show a (brief) MHD-quietescent phase, where FILD was still measuring fast-ion losses with no specific frequency.

• SS beam

For the SS beam, experimental data from shot #47132 have been used. #47132 is a high-performance shot with a plasma current $I_p = 750$ kA and a magnetic field at the magnetic axis of $B_t = 0.65$ T. The main injection energy for this shot was $E_{SS} = 62.8$ keV, with an input power of 1.5 mW. The magnetics spectrogram obtained from the outboard Mirnov array for high-frequency acquisition (OMAHA) coils [43] is presented in figure 11(a), along with the spectrogram of the fast-ion losses measured by FILD in figure 11(b). These spectrograms were used to select the time instant for this analysis, shown by the dashed pink line: $t = 0.3$ s. This time point is within the time windows mentioned before, where there are very brief periods where the modes (in this case, toroidal Alfvén

eigenmodes and fishbones) are not present in the magnetics spectrogram, and FILD is still measuring fast-ion losses with no specific frequency, as can be observed by the signal at the bottom of figure 11(b), with 0 Hz frequency.

A raw frame captured by the new XIMEA camera corresponding to the time of interest, $t = 0.3$ s, is displayed in figure 12, with a superimposed strike map calculated with FIELDSIM. This shows that the measured losses are located at the high pitch-angle area of the scintillator. Moreover, the spots are centered at the same gyroradius. The remap to pitch angle—gyroradius phase space in figure 13 reveals that the losses do not exhibit a single pitch angle, with four distinguishable spots. In the case where only prompt losses are being measured, the gyroradius at the peak of the experimental distribution should agree with the gyroradius corresponding to the injection energy of the beam within the resolution of the diagnostic. In this case, the gyroradius of the injected ions was 12.37 cm, calculated with the magnetic field at the pinhole, and is marked in this figure by the pink line.

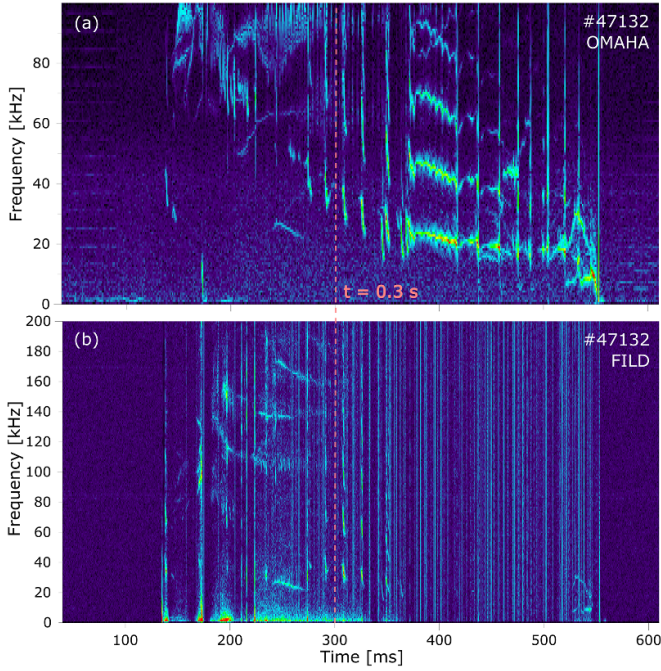


Figure 11. Spectrograms from the OMAHA coils (a) and from FILD (b). The time instant selected for the analysis, $t = 0.3$ s, is shown by the dashed pink line.

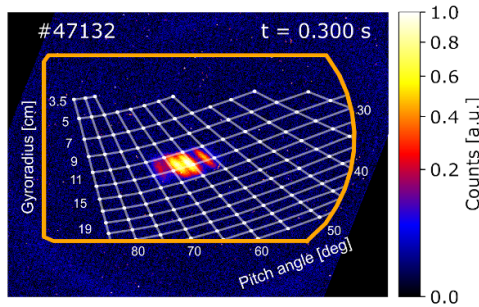


Figure 12. Raw frame from the XIMEA camera at $t = 0.3$ s with a superimposed strike map calculated with FIELDSIM (white), for shot #47132. The orange line shows the contour of the scintillator plate.

It can be observed that the gyroradius measured experimentally is very similar for all four spots, being centered slightly above the beam injection gyroradius. This can be better discerned in figure 14, where the integral in pitch angle has been performed, resulting in a 1D distribution of the experimentally measured gyroradius for this time instant (in blue). The blue line marks the peak of this experimental distribution, at approximately 12.4 cm. Therefore, the experimentally measured gyroradii and the injection gyroradius are in very good agreement, with the resolution of the detector for this range of pitch angle and gyroradius being around 1.5 cm. Furthermore, the synthetic distribution for a 12.4 cm gyroradius ($\lambda = 61$ degrees) calculated with FIELDSIM is depicted in grey, showing a strong match, with the experimental distribution being slightly wider at higher gyroradii.

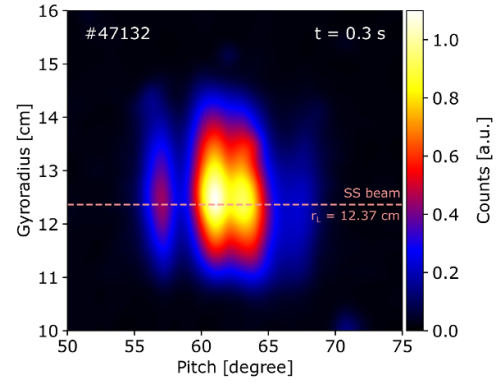


Figure 13. Remap to pitch—gyroradius of the measured losses, showing spots with different pitch angles. The gyroradius corresponding to the injection energy of the beam (12.37 cm) is shown in pink.

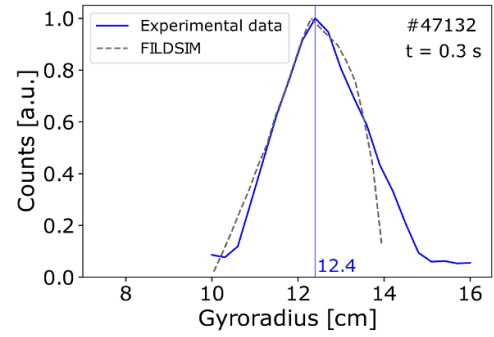


Figure 14. Distribution of the experimentally measured gyroradius (in blue), for shot #47132, at $t = 0.3$ s. The peak is located at 12.4 cm, as marked by the blue line. The FIELDSIM predicted distribution for $r_L = 12.4$ cm, $\lambda = 61$ degrees is shown by the grey dashed line.

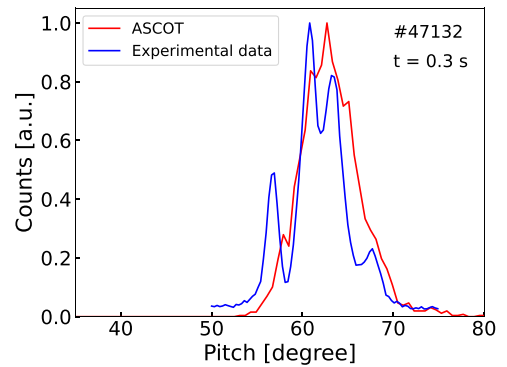


Figure 15. Comparison between the ASCOT simulation (red) and the experimental measurement (blue) of the pitch distribution of the losses reaching the FILD probe, for shot #47132, at $t = 0.3$ s.

Moreover, the pitch of the losses measured by FILD during the analysed time instant is compared against the ASCOT prediction in figure 15, showing a fairly good agreement. For this simulation, experimental data from TS and CXRS have been used, along with the MSE-constrained reconstructed magnetic

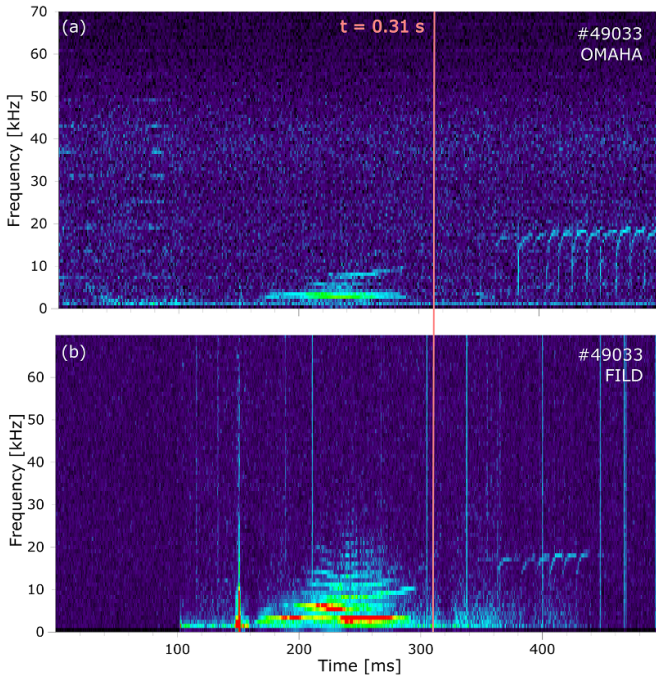


Figure 16. Spectrograms from the OMAHA coils (a) and from FILD (b). The time instant selected for the analysis, $t = 0.31$ s, is shown by the dashed pink line.

equilibrium. Furthermore, a realistic 3D wall with FILD located at the experimental radial position and orientation has been used. The small discrepancy is most probably due to the uncertainties in the inputs used for the ASCOT simulations. In particular, the fit performed to the experimental data of the kinetic profiles has a great impact on the deposition profile calculated with ASCOT, which greatly affects the synthetic FILD signal. Furthermore, the experimental data of the electron density at the scrape-off-layer is scarce, having an impact on this fit.

• SW beam

For the SW beam, experimental data from shot #49033 have been used. #49033 is an L-mode shot with a plasma current $I_p = 750$ kA and a magnetic field at the magnetic axis of $B_t = 0.6$ T. The main injection energy for this shot was $E_{SW} = 52.4$ keV, with an input power of 1 mW. The process to select the time instant for the analysis is analogous to the one followed for the SS beam. The spectrograms from the OMAHA coils (a) and FILD (b) are displayed in figure 16, respectively, for the first half of the shot. In this discharge, the MHD-free period is more clear, from ~ 0.3 to ~ 0.35 s, where FILD is still measuring fast-ion losses with no specific frequency. In this case, the time instant selected was $t = 0.31$ s due to the availability of the TS data.

A raw frame corresponding to the time of interest, $t = 0.31$ s, is displayed in figure 17, with the strike map calculated with FIELDSIM. In this case, the measured losses are mainly located at the low pitch-angle area of the scintillator, with the spots being centered at a specific gyroradius. Similar to the

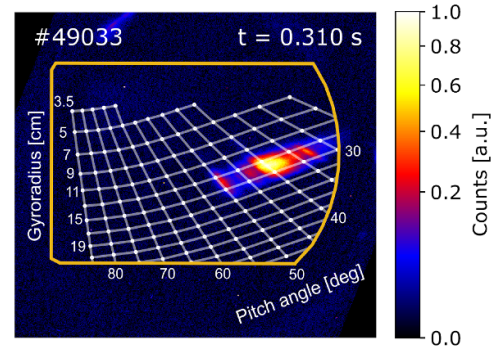


Figure 17. Raw frame from the XIMEA camera at $t = 0.31$ s, for shot #49033, with the corresponding strike map. The orange line shows the contour of the scintillator plate.

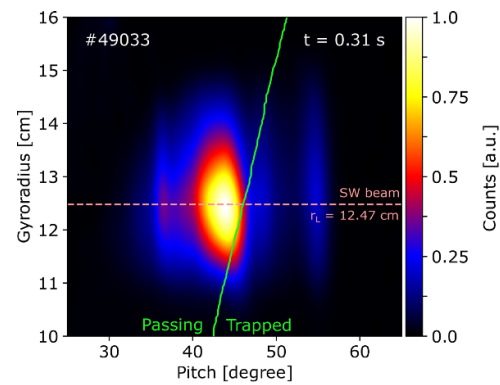


Figure 18. Remap to pitch—gyroradius of the measured losses, showing spots with different pitch angles. The gyroradius corresponding to the injection energy of the beam is shown in pink, 12.47 cm. The trapped-passing boundary is depicted in green.

SS beam scenario, the remap to pitch angle—gyroradius in figure 18 reveals that the losses do not exhibit a single pitch angle, with at least four distinguishable spots. The trapped-passing boundary is depicted in green, suggesting that both passing and trapped particles are being measured. In this scenario, due to the lower magnetic field, the 52.4 keV of injection energy corresponds to 12.47 cm, as marked by the pink line. In this case, the peak of the distribution is located at approximately 12.4 cm, as can be better observed in figure 19. Once again, the agreement between the experimentally measured gyroradii and the injection gyroradius is very good and within the resolution of the detector for this range of pitch angle and gyroradius (around 1.3 cm). The synthetic distribution for the 12.5 cm gyroradius ($\lambda = 44$ degrees) is depicted in grey, showing a strong match. Finally, the comparison of the distribution of the pitch angle of the measured losses against the ASCOT prediction is shown in figure 20. In this case, two main spots are measured experimentally (blue line), centered at 44 and 55 degrees. For a gyroradius of 12.5 cm, the trapped-passing boundary is located at $\lambda \sim 46$ degrees, as shown in figure 18. This means that most of the losses measured in this frame correspond to passing orbits ($\lambda < 46$ degrees), while the peak at

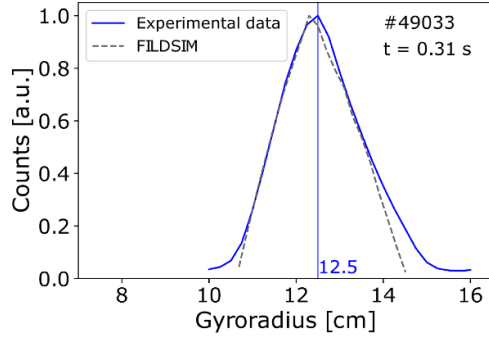


Figure 19. Distribution of the experimental gyroradius (in blue), for shot #49033, at $t = 0.31$ s. The peak is located at 12.5 cm, as marked by the blue line. The FILDSIM predicted distribution for $r_L = 12.5$ cm and $\lambda = 44$ degrees is shown by the grey dashed line.

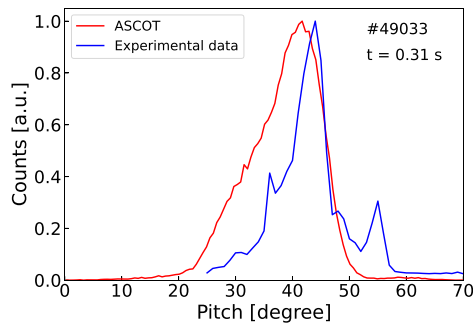


Figure 20. Comparison between the ASCOT simulation (red) and the experimental measurement (blue) of the pitch distribution of the losses, for shot #49033, at $t = 0.31$ s. The dashed vertical lines mark the pitch angles of the respective peaks.

55 degrees corresponds to trapped particles. The pitch distribution predicted by ASCOT (red line) for the SW beam is wider than the experimental distribution, and the peak at 44 degrees is shifted by 2 degrees to lower pitch angles. The experimental spot located at 55 degrees is only reproduced by the tail in the ASCOT distribution at around 60 degrees. Therefore, it seems that ASCOT predicts a lower pitch angle for passing particles, while predicting a higher pitch angle for trapped particles. Since only the SW beam was used in this experiment, there was no CXRS nor MSE data, so the assumption $T_i = T_e$ has been made, and the equilibrium used is not MSE-constrained, but only constrained by magnetics data, which increases the uncertainty of the reconstructed q profile. These are possible causes for the disparities in the pitch distribution, in addition to the fit of the kinetic profiles discussed for the SS scenario.

6. Type-III ELM-induced fast-ion losses

As it was previously introduced, a high-speed CMOS camera was installed for the second campaign, with an acquisition frequency of up to 3.5 kHz. This made it possible to measure type-III ELM-induced losses with the FILD for the first time in MAST-U. The velocity-space of the induced losses

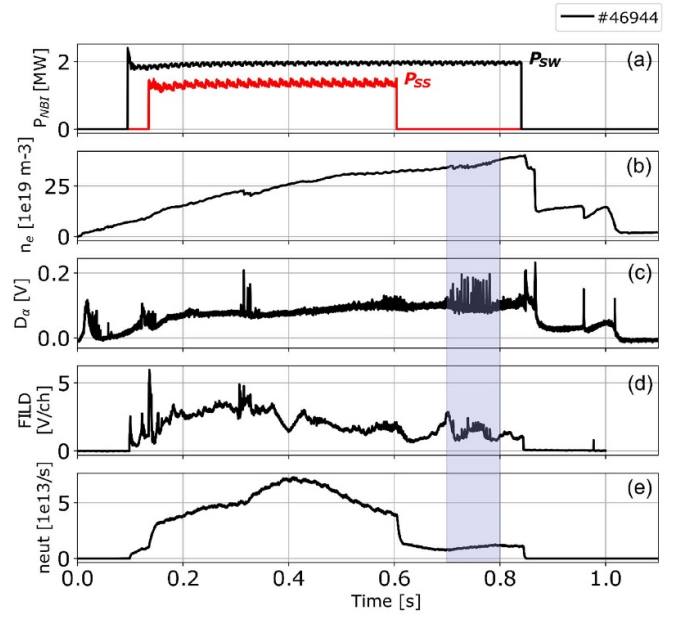


Figure 21. Time traces of the relevant signals for discharge #46944, showing the evolution throughout the discharge of the NBI power (a—SW in black, SS in red), line-integrated electron density (b), D_α (c), integrated FILD signal (d) and neutrons measured with the fission chamber (e). The purple section marks the time window of interest for the type-III ELM analysis.

is analysed in this section, using the high-performance discharge #46944, with $I_p = 750$ kA and $B_t = 0.66$ T on axis. The FILD detector had a measuring range in pitch covering from 20 to 85 degrees. The relevant time traces of this discharge are displayed in figure 21: input power of each of the beams, where the SW is shown in black and the SS in red; evolution of the line-integrated electron density, that again was not feedback-controlled and hence kept increasing during the discharge; the D_α emission; the integrated signal measured by the FILD detector with the APD camera and finally the neutron rate measured with the fission chamber. As it is shown in this figure, both beams were on for the majority of the discharge, but the SS beam was turned off at $t = 0.6$ s. The analysis here will focus on the time window marked in purple in this image, from $t = 0.7$ s to $t = 0.8$ s, where only the SW beam was on with 2 mW of input power and 73 keV of injection energy. As indicated by the peaks in the D_α emission, this is the region where the type-III ELMs appear [44], with a frequency of about 200 Hz and when the electron temperature at the pedestal is below 150 eV. Figure 22 shows a zoom at this time window of interest, for the last four mentioned signals. As it can be seen in this figure, there are peaks in the FILD signal correlated with the ELMs, marked by the peaks in the D_α emission. It can be observed that this enhancement of fast-ion losses is not correlated with drops in the neutron emission measured by the fission chamber, indicating that the ELMs have only a small effect on the global fast-ion confinement, and therefore most fast-ion losses measured by the FILD detector are coming from the plasma edge.

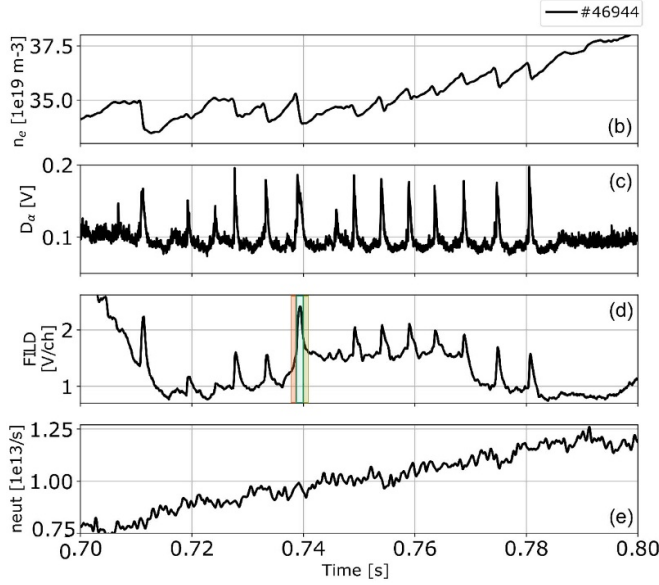


Figure 22. Zoom on time traces (b)–(e) in figure 21, during the time window marked in purple. The orange, green and yellow sections in the FILD signal mark the time points selected for the velocity-space analysis.

By applying the velocity-space analysis techniques discussed in the previous section, it is possible to experimentally resolve the velocity-space of the measured ELM-induced losses, allowing the subsequent analysis of the topology of the orbits through ASCOT modelling. Figure 23 shows the remap to pitch and gyroradius for the time points marked in orange, green and yellow in figure 22: $t = 0.737$ s, pre-ELM (a), $t = 0.738$ s, during-ELM (b) and $t = 0.74$ s, post-ELM (c), respectively. The frame corresponding to $t = 0.739$ s is not displayed here, as the ELM peak is present for 2 ms and hence it is a very similar frame to that of $t = 0.738$ s. In these figures, the trapped-passing boundary is depicted in green, indicating that all the losses measured follow passing orbits. In the different frames, five spots can be distinguished, localised at pitch angles 33, 36, 38.5, 41 and 47 degrees. This is more clearly shown in figure 24, where the 1D distribution in pitch angle has been calculated by integrating in the gyroradius direction. As it can be observed in figure 25, all these spots show a similar increase in intensity, of $\sim 25\%$ – 30% , correlated with the ELMs. For an easier comparison, the time traces shown in this figure correspond to the intensity of the different pitch ranges identified, normalised to the maximum number of counts that each spot reaches in the displayed time window. The gyroradius at which each of the spots peaks can also be identified by integrating in the different pitch ranges that can be discerned in figure 24 for the different spots: [30, 34] for 33 degrees, [34.8, 36.5] for 36 degrees, [36.9, 40] for 38.5 degrees, [40, 42.5] for 41 degrees and [45.5, 48.5] for 47 degrees. The result is shown in figure 26. As it was already visible from the overall view of the velocity-space presented in figure 23, the peak in gyroradius is very similar for all the spots being analysed. Figure 26 shows that, specifically, all three spots corresponding to 38, 41

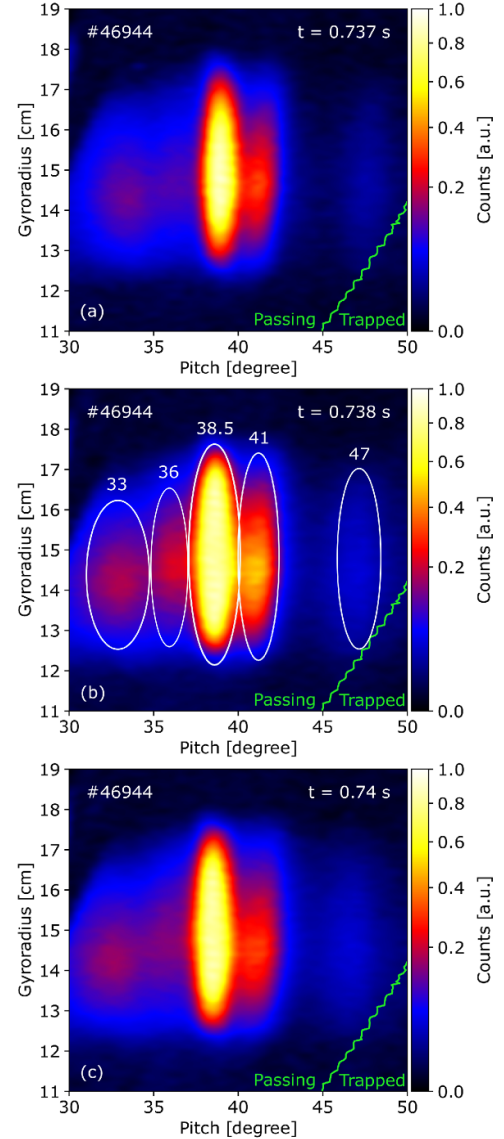


Figure 23. Remap to pitch—gyroradius of the losses measured by FILD in discharge #46944 during an ELM cycle: (a) $t = 0.737$ s, pre-ELM, (b) $t = 0.738$ s, during ELM and (c) $t = 0.74$ s, post-ELM. The trapped-passing boundary is shown in green. The main pitch angles are identified in white for $t = 0.738$ s.

and 47 degrees peak at the same gyroradius: 14.4 cm, while the other two, corresponding to 33 and 36 degrees, peak at 14.1 and 14.7 cm, respectively. As it was previously mentioned, the SW beam injection energy for this shot was 73 keV. When converted to gyroradius, this corresponds to 14.32 cm at the FILD pinhole. For the range of pitch and gyroradius analysed here, the resolution would be of approximately 1.7 cm. Therefore, the experimental values obtained are within the resolution of the detector, which would indicate that the effect of the ELMs is purely in terms of the increase in the signal shown in figure 25. In conclusion, the analysis indicates that ELMs have a clear effect on the fast-ions, resulting in an enhancement of fast-ion losses of $\sim 25\%$ – 30% , with no particular preference in velocity-space.

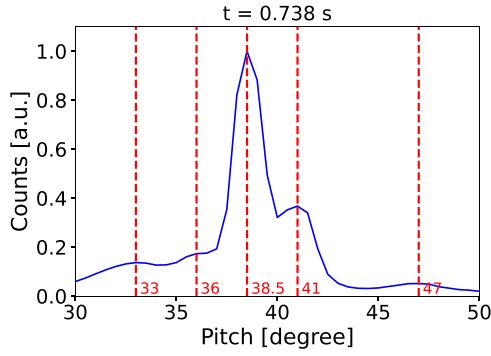


Figure 24. 1D distribution of the pitch angle of the losses measured by FILD, showing the different spots, identified at 33, 36, 38.5, 41 and 47 degrees, during the ELM peak ($t = 0.738$ s).

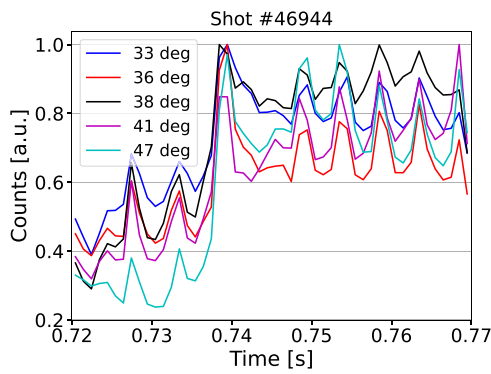


Figure 25. Time traces of the intensity of the main spots, identified at 33, 36, 38.5, 41 and 47 degrees during the ELM peak, each normalised to their maximum number of counts in the displayed time window.

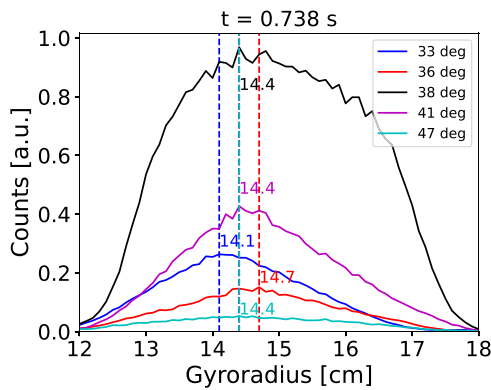


Figure 26. 1D distribution in gyroradius obtained by integrating in the five pitch ranges identified during the ELM peak for the different spots under analysis: [30, 34] for 33 degrees, [34.8, 36.5] for 36 degrees, [36.9, 40] for 38.5 degrees, [40, 42.5] for 41 degrees and [45.5, 48.5] for 47 degrees.

The information retrieved through this velocity-space analysis allows us to resolve the orbits of the losses, that can be traced back using the ASCOT code. This is done by launching the markers from the FILD pinhole backwards, with the energy and pitch angle measured experimentally. In this case, five orbits were followed, corresponding to the five identified

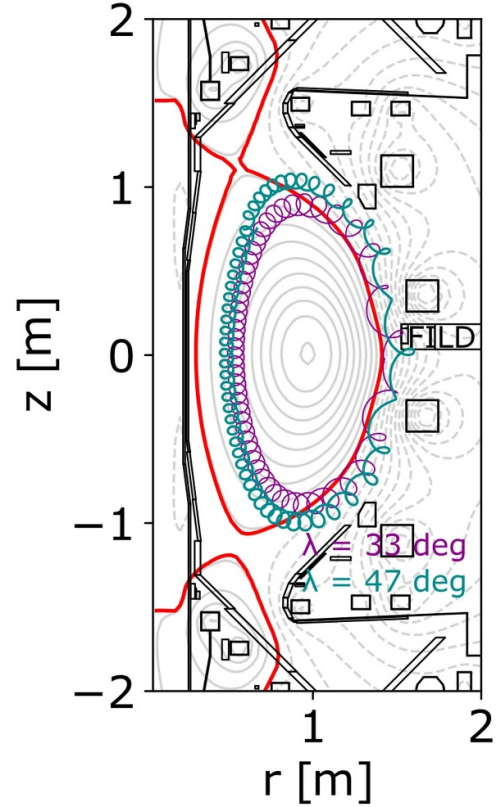


Figure 27. Poloidal cross-section of the MAST Upgrade tokamak with the FILD detector at the radial position of the pinhole during discharge #46944, showing the separatrix in red and the orbit corresponding to the two most extreme pitch angles measured at $t = 0.738$ s: 33 degrees in purple and 47 degrees in blue.

pitch angles: 33, 36, 38.5, 41 and 47 degrees. As for the energy, 73 keV will be used for all the cases. In figure 27, only the two orbits corresponding to the most extreme pitch angles, 33 and 47 degrees, are displayed (purple and blue, respectively). It is possible to observe that they both correspond to passing orbits, as is also the case for the other three that are not shown in the figure for clarity. This is consistent with the trapped-passing boundary that was presented in figure 23.

7. Summary

A new CMOS camera has been successfully installed and operated at the MAST-U FILD, capable of capturing data at an acquisition frequency of up to 3.5 kHz, improving the capabilities of the detector, and making it possible to analyse the velocity-space of the fast-ion losses induced from perturbations and instabilities on a wide variety of time scales, from resonant magnetic perturbations to ELMs.

The commissioning of the diagnostic has been performed through the analysis of two different parameters that directly affect the MAST-U FILD signal: the radial position and the effect of the edge safety factor (q_{95}), respectively. Simulations predicted an inverse relation between the intensity of the FILD signal and its relative distance to the separatrix, with no other plasma facing component obstructing the FILD detection. This

prediction has been validated experimentally by means of a systematic scan in the distance between the FILD probe head and the separatrix. This scan has also shown that the optimal FILD measurement position is around 10 cm, slightly depending on the discharge parameters. With regards to the edge safety factor, simulations predicted a great impact of the q_{95} on the toroidal deposition of the prompt losses, and therefore it was expected to be correlated to the intensity of the FILD signal. The experimental toroidal field ramp performed was a success in terms of scenario development, as it was the first time this was achieved in MAST-U, and also resulted in the expected increase in the FILD signal correlated with a decrease in the edge safety factor, supporting the predictions performed with ASCOT. Experimental efforts are foreseen to be carried out in the next experimental campaign, when it will be possible to run plasmas at a higher plasma current, which would allow us to explore the other possible approach to further reduce the q_{95} .

The experimental resolution of the MAST-U FILD detector has been evaluated for a typical alignment, and shown to be in the order of 0.5 to 1 degree in pitch, and of 1 to 3 cm in gyroradius, both depending on the range of pitch and gyroradius measured. Furthermore, the first analysis of the velocity-space of the losses measured with the MAST-U FILD presented here represents a major achievement. For this analysis, two discharges where each of the beams were used individually were selected, by looking at the MHD-activity in them and selecting those that had the most MHD-quiescent time windows in the FILD database. This facilitates the understanding and validation of the analysis, as the losses measured by FILD in these time windows can be assumed to be prompt losses directly coming from the NBI, with an energy corresponding to the NBI injection gyroradius, and reproducible with ASCOT. The gyroradius measured with FILD agrees with that injected by the beams well within the resolution of the detector for both the SS and SW scenarios. The resolved pitch distribution has been compared against the ASCOT prediction, showing a good agreement in the case of the SS beam, whereas the SW scenario presents a rigid shift of around 7–8 degrees with respect to the ASCOT prediction. This is most probably related to the uncertainties in the inputs used for the ASCOT simulations: For the SW scenario, the equilibrium reconstruction is not MSE-constrained, and is only constrained by magnetics measurements, which can have a big effect in a ST. And, for both cases analysed, the fit performed to the experimental data of the kinetic profiles, which affects the deposition profile calculated with ASCOT, having a direct impact on the synthetic FILD signal. The effect of the fit to the kinetic profiles will be addressed in a future publication, where a more systematic analysis will be presented. The importance of using a MSE-constrained equilibrium is also a key outcome of this study, and will be tackled in the future by including blips of the SS beam as diagnostic beam during the experiments.

Finally, the tools developed for the velocity-space analysis have been applied to the first measurements of type-III ELM-induced losses measured by FILD in MAST-U. This has made it possible to resolve the orbits of the different spots

identified, corresponding to losses with different pitch angles. The analysis shows that the ELMs have a clear effect on the fast-ions, resulting in an enhancement of fast-ion losses of ~25%–30%, with no particular preference in velocity-space, and that all losses reaching the FILD detector come from passing orbits.

In conclusion, this manuscript presents significant progress in fast-ion diagnostics in the context of STs, with an overall agreement between the experimental results and the numerical predictions, validating the predictive capabilities of the simulation models used. The successful installation and exploitation of a high-speed CMOS camera, the optimised measurement position of the FILD detector, the understanding of the effect of the plasma edge safety factor, and the velocity-space analysis of the measured losses, first performed with prompt losses and finally applied to a scenario with ELM-induced losses, provide new tools to further understand fast-ion behaviour in STs. The analysis performed here is key for future fast-ion experiments in MAST-U, where the dynamics of the losses will be investigated in the presence of different types of perturbations: understanding the effect of externally applied magnetic perturbations will be the main line of future research, along with fast-ion losses induced by Alfvén eigenmodes and type-I ELMs-induced losses. Moreover, the understanding of the effect of the edge safety factor, and the optimisation of the FILD measurement of prompt losses coming from the SS beam sets the foundation for the application of the light ion beam probe technique [26, 45] in MAST-U.

Data availability statement

The data generated and/or analysed during the current study are not publicly available for legal/ethical reasons but are available from the corresponding author upon reasonable request.

Acknowledgments

This work has been carried out within the framework of the EUROfusion Consortium, funded by the European Union via the Euratom Research and Training Programme (Grant Agreement No. 101052200—EUROfusion) and from the EPSRC [Grant No. EP/W006839/1]. Views and opinions expressed are however those of the author(s) only and do not necessarily reflect those of the European Union or the European Commission. Neither the European Union nor the European Commission can be held responsible for them. This research received funding from the Plan Andaluz de Investigación, Desarrollo e Innovación (PAIDI 2020, No. 003456/A02W), Consejería de Transformación Económica, Industria, Conocimiento y Universidades de la Junta de Andalucía. This project has received funding from the European Research Council (ERC) under the European Union's Horizon 2020 research and innovation programme (Grant Agreement No. 805162). J Galdon-Quiroga acknowledges support from the MSCA PF programme under Grant


No. 101069021. The simulations were partly performed on the MARCONI supercomputer (CINECA).

ORCID iDs

Lina Velarde  <https://orcid.org/0000-0002-3986-1583>

J F Rivero-Rodríguez  <https://orcid.org/0000-0001-5074-0267>

J Galdón-Quiroga  <https://orcid.org/0000-0002-7415-1894>

J Rueda-Rueda  <https://orcid.org/0000-0002-4535-326X>

P Cano-Megías  <https://orcid.org/0000-0001-5182-6513>

M García-Muñoz  <https://orcid.org/0000-0002-3241-502X>

K G McClements  <https://orcid.org/0000-0002-5162-509X>

L Sanchís  <https://orcid.org/0000-0001-8211-3356>

E Viezzer  <https://orcid.org/0000-0001-6419-6848>

References

- [1] Berkery J W, Xia G, Sabbagh S A, Bialek J M, Wang Z R, Ham C J, Thornton A and Liu Y Q 2020 Projected global stability of high beta mast-u spherical tokamak plasmas *Plasma Phys. Control. Fusion* **62** 085007
- [2] Costley A E and McNamara S A M 2021 Fusion performance of spherical and conventional tokamaks: implications for compact pilot plants and reactors *Plasma Phys. Control. Fusion* **63** 035005
- [3] Fasoli A *et al* 2007 Chapter 5: physics of energetic ions *Nucl. Fusion* **47** S264
- [4] Keeling D L *et al* (the MAST Team) 2014 Mitigation of MHD induced fast-ion redistribution in mast and implications for mast-upgrade design *Nucl. Fusion* **55** 013021
- [5] Galdón-Quiroga J *et al* 2018 Velocity space resolved absolute measurement of fast ion losses induced by a tearing mode in the ASDEX Upgrade tokamak *Nucl. Fusion* **58** 036005
- [6] Pinches S D, Chapman I T, Lauber P W, Oliver H J C, Sharapov S E, Shinohara K and Tani K 2015 Energetic ions in ITER plasmas *Phys. Plasmas* **22** 021807
- [7] Michael C A *et al* 2013 Dual view FIDA measurements on MAST *Plasma Phys. Control. Fusion* **55** 095007
- [8] Prechel G, Fil N, Liu D, Heidbrink W W, Michael C, Jackson A R and Team M A S T-U 2022 Installation of a solid state neutral particle analyzer array on mega ampere spherical tokamak upgrade *Rev. Sci. Instrum.* **93** 113517
- [9] Ceconello M *et al* (the MAST-Uteam) 2023 First observations of confined fast ions in MAST Upgrade with an upgraded neutron camera *Plasma Phys. Control. Fusion* **65** 035013
- [10] Perez R V *et al* 2014 Investigating fusion plasma instabilities in the mega amp spherical tokamak using mega electron volt proton emissions (invited) *Rev. Sci. Instrum.* **85** 11D701
- [11] Zweben S J 1989 Pitch angle resolved measurements of escaping charged fusion products in TFTR *Nucl. Fusion* **29** 825
- [12] Baeumel S *et al* (JET-EFDA Contributors) 2004 Scintillator probe for lost alpha measurements in JET *Rev. Sci. Instrum.* **75** 3563–5
- [13] García-Muñoz M, Fahrbach H U and Zohm H 2009 Scintillator based detector for fast-ion losses induced by magnetohydrodynamic instabilities in the ASDEX Upgrade tokamak *Rev. Sci. Instrum.* **80** 053503
- [14] Darrow D *et al* (JET-EFDA Contributors) 2006 Initial results from the lost alpha diagnostics on Joint European Torus *Rev. Sci. Instrum.* **77** 10E701
- [15] Kiptily V G *et al* (JET-EFDA Contributors) 2009 Recent progress in fast ion studies on JET *Nucl. Fusion* **49** 065030
- [16] Rivero-Rodríguez J F *et al* (JET Contributors) 2021 Upgrade and absolute calibration of the JET scintillator-based fast-ion loss detector *Rev. Sci. Instrum.* **92** 043553
- [17] Fisher R K, Pace D C, García-Muñoz M, Heidbrink W W, Muscatello C M, Van Zeeland M A and Zhu Y B 2010 Scintillator-based diagnostic for fast ion loss measurements on DIII-D *Rev. Sci. Instrum.* **81** 10D307
- [18] Ayllón-Guerola J *et al* 2021 Thermo-mechanical assessment of the JT-60SA fast-ion loss detector *Fusion Eng. Des.* **167** 112304
- [19] Ogawa K *et al* 2019 Energy-and-pitch-angle-resolved escaping beam ion measurements by faraday-cup-based fast-ion loss detector in Wendelstein 7-X *J. Instrum.* **14** C09021
- [20] van Vuuren A J, Lazerson S A, LeViness A, García-Muñoz M, Gates D, Quiroga J G, Hidalgo-Salaverri J, Rueda-Rueda J, García-Domínguez J and Ayllón Guerola J M 2022 Conceptual design of a scintillator-based fast-ion loss detector for the Wendelstein 7-X stellarator *IEEE Trans. Plasma Sci.* **50** 4114–9
- [21] Rivero-Rodríguez J F *et al* 2018 A rotary and reciprocating scintillator based fast-ion loss detector for the MAST-U tokamak *Rev. Sci. Instrum.* **89** 10I112
- [22] Rivero-Rodríguez J F, Velarde L, Williams T, Galdón-Quiroga J, García-Muñoz M and McClements K G 2024 Initial operation of the scintillator-based fast-ion loss detector rotary and reciprocating system in MAST-U *IEEE Trans. on Plasma Science* pp 1–0
- [23] Rivero-Rodríguez J F *et al* (the EUROfusion Tokamak Exploitation Team and the MAST-U Team) 2024 Overview of fast particle experiments in the first mast upgrade experimental campaigns *Nucl. Fusion* **64** 086025
- [24] Gonzalez-Martin J *et al* 2019 First measurements of a magnetically driven fast-ion loss detector on ASDEX Upgrade *J. Instrum.* **14** C11005
- [25] Darrow D S, Bäuml S, Cecil F E, Kiptily V, Ellis R, Pedrick L and Werner A 2004 Design and construction of a fast ion loss Faraday cup array diagnostic for Joint European Torus *Rev. Sci. Instrum.* **75** 3566–8
- [26] Chen X *et al* 2014 Using neutral beams as a light ion beam probe *Rev. Sci. Instrum.* **85** 11E701
- [27] Hirvijoki E, Asunta O, Koskela T, Kurki-Suonio T, Miettunen J, Sipilä S, Snicker A and Äkäslompolo S 2014 ASCOT: solving the kinetic equation of minority particle species in tokamak plasmas *Comput. Phys. Commun.* **185** 1310–21
- [28] Velarde L 2021 Neutral beam injector design for the SMAll Aspect Ratio Tokamak (SMART) of the university of seville
- [29] Asunta O, Govenius J, Budny R, Gorelenkova M, Tardini G, Kurki-Suonio T, Salmi A and Sipilä S 2015 Modelling neutral beams in fusion devices: beamlet-based model for fast particle simulations *Comput. Phys. Commun.* **188** 33–46
- [30] Peng Q, Ferron J R, Strait E J, Taylor T S, Meyer W H, Zhang C, Lao L L, John H E and You K I 2005 MHD equilibrium reconstruction in the DIII-D tokamak *Fusion Sci. Technol.* **48** 968–77
- [31] Scannell R, Walsh M J, Carolan P G, Conway N J, Darke A C, Dunstan M R, Hare D and Prunty S L 2006 Enhanced edge Thomson scattering on MAST *Rev. Sci. Instrum.* **77** 10E510
- [32] Wisse M 2007 Charge-exchange spectroscopy in the MAST tokamak *PhD Thesis*
- [33] Ayllón-Guerola J *et al* 2019 Determination of the fast-ion phase-space coverage for the FILD spatial array of the ASDEX Upgrade tokamak *J. Instrum.* **14** C10032
- [34] Gonzalez-Martin J *et al* (ASDEX Upgrade Team and MST1 Team) 2021 Self-adaptive diagnostic of radial fast-ion loss

- measurements on the ASDEX Upgrade tokamak (invited) *Rev. Sci. Instrum.* **92** 053538
- [35] Costley A E 2019 Towards a compact spherical tokamak fusion pilot plant *Phil. Trans. R. Soc. A* **377** 20170439
- [36] Kogan L *et al* (the MAST-Uteam) 2022 First MAST-U equilibrium reconstructions using the EFIT++ code *Proc. 48th EPS Conf. on Plasma Physics* (European Physical Society)
- [37] Cecconello M, Sperduti A, Fitzgerald I, Conroy S, Holm S J and Weiszflog M 2018 The neutron camera upgrade for MAST Upgrade *Rev. Sci. Instrum.* **89** 10I110
- [38] Rueda-Rueda J *et al* 2024 Joseruedarueda/ufildsim: v4.4 *Zenodo* (available at: <https://zenodo.org/records/5849643>)
- [39] Rueda-Rueda J *et al* (ASDEX Upgrade Team) 2024 Commissioning of the imaging neutral particle analyser for the ASDEX Upgrade tokamak *Plasma Phys. Control. Fusion* **66** 035008
- [40] Galdón-Quiroga J *et al* 2018 Velocity-space sensitivity and tomography of scintillator-based fast-ion loss detectors *Plasma Phys. Control. Fusion* **60** 105005
- [41] Oyola P *et al* (ASDEX Upgrade Team) 2021 Implementation of synthetic fast-ion loss detector and imaging heavy ion beam probe diagnostics in the 3D hybrid kinetic-MHD code MEGA *Rev. Sci. Instrum.* **92** 043558
- [42] Boris J P 1971 *Relativistic Plasma Simulation—Optimization of a Hybrid Code* vol AD-A023 (Naval Research Laboratory) p 511
- [43] Hole M J, Appel L C and Martin R 2009 A high resolution Mirnov array for the mega ampere spherical tokamak *Rev. Sci. Instrum.* **80** 123507
- [44] Kirk A, O’Gorman T, Saarelma S, Scannell R and Wilson H R (the MAST team) 2009 A comparison of H-mode pedestal characteristics in MAST as a function of magnetic configuration and ELM type *Plasma Phys. Control. Fusion* **51** 065016
- [45] Galdon-Quiroga J *et al* (the ASDEX Upgrade Team and the EUROfusion MST1 Team) 2022 Experimental investigation of beam-ion losses induced by magnetic perturbations using the light ion beam probe technique in the ASDEX Upgrade tokamak *Nucl. Fusion* **62** 096004